Korean J. Chem. Eng., 39(5), 1227-1231 (2022)
DOI: 10.1007/s11814-022-1060-0

pISSN: 0256-1115
eISSN: 1975-7220

Optimization of high-energy ball milling process for uniform p-type Bi-Sb-Te thermoelectric material powder

Hye Jin Im*, Bokun Koo*, Min-Soo Kim*, and Ji Eun Lee,†**

*Energy Conversion Research Center, Korea Electrotechnology Research Institute, Changwon 51543, Korea
**School of Chemical Engineering, Chonnam National University, Gwangju 61186, Korea
(*Received 16 July 2021 • Revised 17 December 2021 • Accepted 2 January 2022*)

Abstract−Ball milling is widely used for producing powders of thermoelectric materials owing to its simplicity and scalability. In this research, we investigated the particle shape and size in p-type Bi-Sb-Te materials—the best-known and only commercially available thermoelectric materials at present—after high-energy ball milling. Although Bi-Sb-Te materials are known to be brittle, some ductile properties, such as particle agglomeration and welding, were observed. To avoid an increase in particle size via welding and to obtain particles with highly uniform sizes, two-step ball milling was performed and particle sizes were analyzed. The ball-milled powder was consolidated and sintered, and the resulting pellets showed no crystallographic orientation and consequently exhibited uniform thermal and electrical conductivities regardless of measurement direction.

Keywords: Ball Mill, Bi-Sb-Te, Thermoelectric, Cold Welding

INTRODUCTION

Research on energy harvesting technologies has garnered intensive interest owing to energy and environmental issues. Among them, thermoelectric technologies, which directly convert thermal energy to electrical energy and vice versa via the Seebeck effect, are gaining substantial interest based on their applications in waste-heat recovery and refrigeration [1,2]. The energy conversion efficiency of thermoelectric materials is characterized by the figure of merit, $ZT=S^2\sigma T/\kappa$, where S is the Seebeck coefficient, σ is the electrical conductivity, T is the absolute temperature, and κ is the thermal conductivity. A higher value of ZT corresponds to a higher energy conversion efficiency. For good efficiency, materials with high electrical conductivity, low thermal conductivity, and a high Seebeck coefficient are needed; however, it is difficult to achieve high ZT values owing to the interrelationships between electrical and thermal properties [3]. Recently, it has been reported that nanostructured bulk thermoelectric materials show reduced thermal conductivity and improved ZT caused by phonon scattering at grain boundaries and interfaces [4,5]. Nanostructured bulk thermoelectric materials are generally manufactured by sintering fine powder called powder metallurgy [4-7]. In this manufacturing method, properties of the powder, such as composition and size, affect the sintering process and the resulting sintered ingot [8,9].

Meanwhile, fabrication of thermoelectric devices by printing has been actively researched [10,11]. Unlike conventional thermoelectric device fabrication, dicing ingots into mm-sized pellets and typically sandwiching them between two ceramic plates, printing is low-cost, low material waste and flexible substrates applicable process. Through 3D printing method, thermoelectric generators have been made using SnSe and BiSbTe ink. The ink used for 3D printing is made of powder of thermoelectric materials, and powder size and distribution are important factors in printing process and mechanical strength [12,13].

Preparation of fine powder and control of particle size distribution are critical for both 3D printing and sintering of nanostructured bulk process. Among the various methods of preparing thermoelectric materials in powder form, the ball-milling process is prevailingly employed in solid-state synthesis and powder metallurgy processing owing to its simplicity, potential for easy scale-up, and applicability to all classes of materials. Therefore, in many cases, powders of thermoelectric materials for nanostructured bulk are fabricated via the ball milling process [14,15]. Ball milling involves several parameters, such as milling time, milling speed, ball size, and ball-to-material ratio. Furthermore, ball milling can affect the formation of defects and carrier concentration, but prolonged ball milling can cause undesirable doping [16]. Therefore, studies on the optimization of the ball milling process are meaningful in preparing a better thermoelectric powder.

In low speed ball milling near 300 rpm, it takes a long time, about 10 hours, to obtain a fine and uniform powder [15,16]. By using high energy ball milling, it is expected that the time can be shortened, but there are few studies on this. In this research, we investigated the particle size of Bi-Sb-Te, the best p-type thermoelectric material at room temperature, according to ball milling conditions. Although Bi-Sb-Te materials are known to be brittle, some ductile attributes such as the agglomeration and welding were observed in the high energy ball mill process. To avoid particle enlargement by welding and obtain particles with more uniform sizes, milling time and speed were optimized.

†To whom correspondence should be addressed.
E-mail: jelee@jnu.ac.kr

EXPERIMENTAL PROCEDURES

Here, p-type Bi-Sb-Te ingots (Kryotherm) were used as the staring material. The ingots were broken into small pieces and sealed with zirconia balls in an 80 mL zirconia-lined ball mill jar under an Ar atmosphere. Ball milling was conducted using a planetary Micro Mill premium line (Pulversette 7, Fritsch) at different speeds for different time periods with different sized balls. The ball : ingot weight ratio was 3 : 1. As a control, hand-milled sample was prepared by crushing the ingot with mortar for 1 h. After milling, the powder was loaded into a graphite mold and consolidated via spark plasma sintering (Dr. Sinter, SPS-systex) under an Ar atmosphere for 5 min at 693 K with a pressure of 50 MPa. The dense samples were cut into rectangular pieces for electrical resistivity and Seebeck coefficient measurements and into cylindrical pieces for thermal diffusivity measurements.

Particle size distribution was measured using a particle size analyzer (Mastersizer 2000, Malvern) via the dynamic light scattering (DLS) technique. The size distribution was determined based on the average of five repeated measurements. The phases of the powder and bulk samples were characterized using X-ray diffraction (XRD) analysis (X'pert-Pro MPD, PANalytical), while the microstructures of the samples were investigated using field-emission scanning electron microscopy (FE-SEM, S-4800, Hitachi). The electrical conductivity and Seebeck coefficient values were measured using a commercial ZEM-3 system (ULVAC-RIKO), based on the standard four-probe method. Thermal diffusivity was measured using a laser flash analysis system (LFA 447, Netzsch); further, the thermal conductivity (κ) values were calculated using the equation $\kappa=\rho C_p D$, where ρ is the density, C_p is the specific heat capacity, and D is the thermal diffusivity.

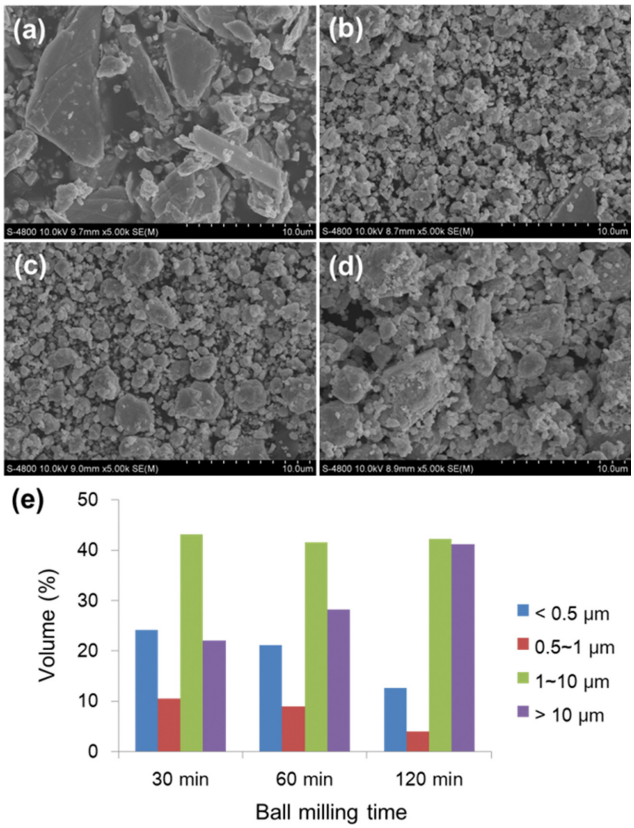

Fig. 1. SEM images of p-type Bi-Sb-Te powders prepared with different milling times. (a) Hand milling, (b) 30 min milling, (c) 60 min milling, and (d) 120 min milling at 800 rpm. (e) Particle size analysis of ball-milled powders at 800 rpm.

RESULTS AND DISCUSSION

The ball milling process involves several complex parameters, including the type of mill, material of the container, milling speed, milling time, ball size, grinding medium, ball-to-material weight ratio, extent of filling the vial, milling atmosphere, process control agent, and milling temperature [14]. In this research, p-type Bi-Sb-Te ingots were crushed into powders using a high-energy planetary ball mill, a common milling system used for thermoelectric materials. Iron contamination was reported when a stainless-steel jar was used [16]; therefore, a zirconia jar and ball were selected, and an inert argon milling atmosphere was employed to avoid oxidization during the process.

Fig. 1(a)-(d) shows the SEM images of a Bi-Sb-Te powder after grinding. A Bi-Sb-Te ingot was ball-milled at high speed, 800 rpm, using large balls of 10 mm in diameter to shorten the milling time. Compared to hand-milled powder (Fig. 1(a)), which has particles that are several tens of micrometers in diameter, the particle size of the ball-milled powder was dramatically reduced to range from several hundred nanometers to a few micrometers. However, as shown in SEM images, prolonged milling leads to an increase in particle size. For quantitative measurement, the particle size of the powders was analyzed via the dynamic light scattering (DLS) technique. Fig. 1(e) shows that the proportion of large particles (>10 μm) increases with milling time. During the milling process, pulverized powder appears to re-aggregate to form large particles.

To closely observe the agglomeration of the powders, high-magnification SEM images were obtained. Fig. 2(a) shows that after ball milling for 30 min, a large particle was composed of numerous small particles, indicating that agglomeration started before 30 min. Agglomeration in the powders also can be confirmed based on the particle size measurements, which show that the proportion of small particles increased with repeated measurements owing to sonication (Fig. 2(c)). After milling for 2 h, the aggregated small particles combined and merged as shown in Fig. 2(b). During high-energy milling, the particles of ductile materials become plastically deformed, flattened, and cold-welded, resulting in plate-like powders [17,18]. Although Bi-Sb-Te materials are known to be brittle, rather than ductile [19], and do not exhibit a plate-like shape during high-energy ball milling, some ductile attributes such as the agglomeration and welding of small particles, which resulted in enlarged particles, were observed. This weak ductility characteristic is consistent with other reports [20] and more revealed at fast ball mill speed due to the high energy. The process of grinding, agglomeration, and welding due to the continuous mechanical milling and possible cumulative heat generation during the high-energy ball milling is illustrated in Fig. 2(d).

To avoid particle enlargement by welding and obtain particles

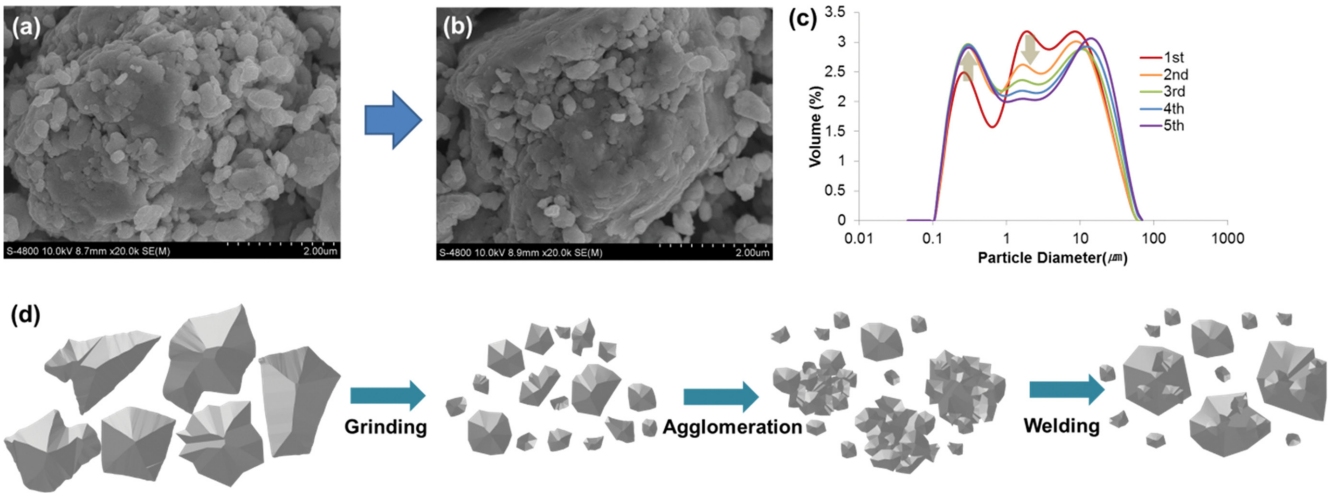

Fig. 2. SEM images of p-type Bi-Sb-Te powders after (a) 30 min milling and (b) 2 h milling. (c) Repeated particle distribution measurement. (d) Illustration of grinding, agglomeration, and welding processes.

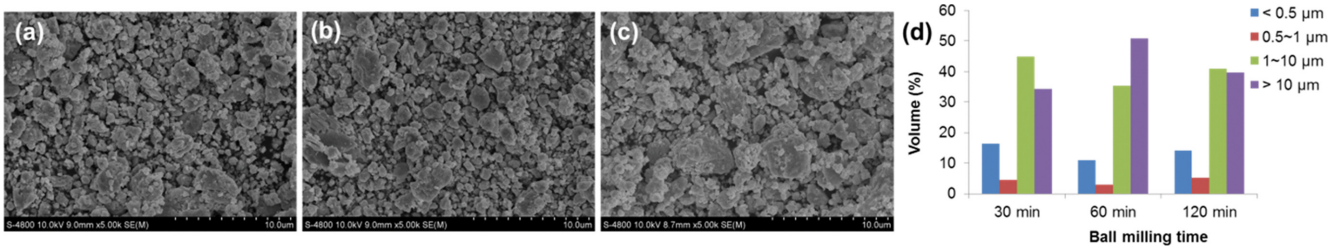

Fig. 3. SEM images of Bi-Sb-Te powders after secondary ball milling step at 300 rpm with small ball (Φ=5 mm) for (a) 30 min, (b) 60 min, and (c) 120 min; (d) Size distribution of ball-milled powder after secondary ball milling step at 300 rpm.

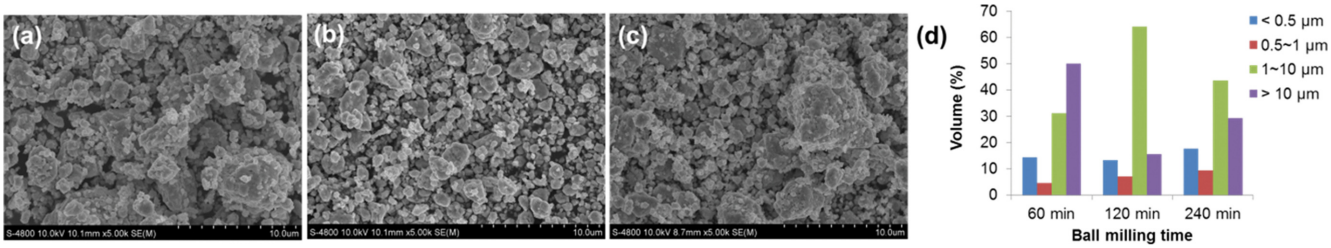

Fig. 4. SEM images of Bi-Sb-Te powders after secondary ball milling step at 150 rpm with small ball (Φ=5 mm) for (a) 60 min, (b) 120 min, and (c) 240 min; (d) Size distribution of ball-milled powder after secondary ball milling step at 150 rpm.

with highly uniform sizes, ball milling using smaller balls at a lower speed was additionally performed using a powder milled at 800 rpm for 30 min with large balls (Φ=10 mm). It was previously reported that substantial variations in powder size can be attributed to ineffective milling due to powders trapped in gaps between large grinding balls and a two-step milling process was effective for obtaining uniform powders [15]. The secondary ball milling process was performed at two different speeds (300 and 150 rpm) using smaller balls (Φ=5 mm) to obtain fine and uniform powders, and the resulting powders are shown in Figs. 3 and 4. Increasing the milling time at a relatively low speed also resulted in the agglomeration of small particles and an increase in particle size; however, the agglomeration rate was reduced with a decrease in milling speed. When secondary ball milling was performed at two different speeds and for different time, the particles milled for 60 min at 150 rpm in the secondary step after first ball mill at 800 rpm for 30 min were the most uniform, as shown in Fig. 4.

The XRD patterns of Bi-Sb-Te powder after hand milling, primary ball milling at 800 rpm for 30 min, and secondary ball milling at 150 rpm for 60 min are shown in Fig. 5. The measured patterns agree with the standard powder diffraction pattern of $Bi_{0.4}Sb_{1.6}Te_3$ (ICDD No. 01-072-1836), and no other decomposed or precipitated phases were found. The strong peaks corresponding to (0 0 *l*), such as (0 0 6) and (0 0 15), in the pattern of the hand-milled sample indicate the existence of a preferred crystallographic orientation (texture) in the material. The texture disappeared as the ingots were ground into a fine powder, causing those peaks to weaken substantially. The repeated fracturing and welding process during ball

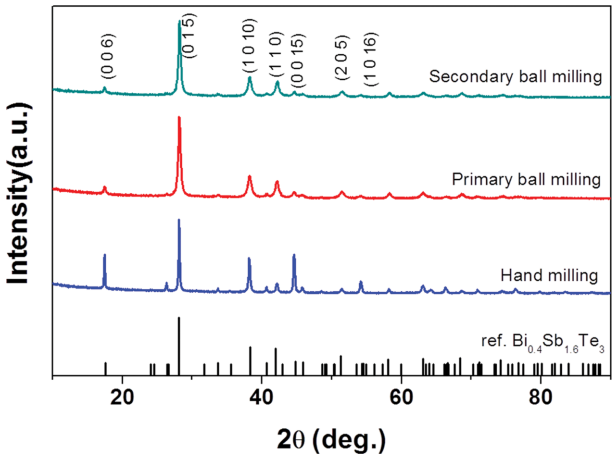

Fig. 5. XRD patterns of Bi-Sb-Te powders after hand milling, primary ball milling, and secondary ball milling.

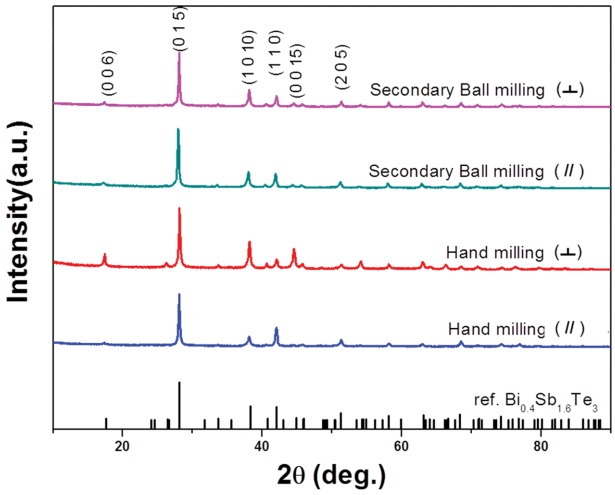

Fig. 6. XRD patterns of sintered bulk Bi-Sb-Te pellets.

milling not only causes a decrease in powder size but also randomizes the powder crystallographic orientation. The peaks of the ball-milled powder were broader than those of the hand-milled one, indicating a decrease in crystal size. When comparing the XRD patterns of the ball-milled powders, there was no significant difference in the patterns according to time or milling speed within our experimental conditions.

The pulverized powders after hand milling and secondary ball milling were sintered via the spark plasma sintering method to obtain high-density pellets. As shown in Fig. 6, for bulk pellets of the hand-milled powder, the XRD diffraction patterns differed depending on the measurement direction. The indexed peaks of (0 0 6) and (0 0 15) are stronger in the diffraction patterns obtained from in-plane surfaces—perpendicular to the pressure axis (⊥)—than those in the patterns obtained from out-of-plane surfaces—parallel to the pressure axis (//); this indicates a c-plane preferred orientation perpendicular to the pressure axis. However, bulk pellets sintered using the ball-milled powder did not exhibit such differences with respect to the measurement direction and preferred orientation.

The measured thermoelectric properties of the sintered materials are presented in Fig. 7. For the sintered pellet prepared from hand-milled powder, the electrical and thermal conductivity depend on measurement direction. They show a higher value in the direc-

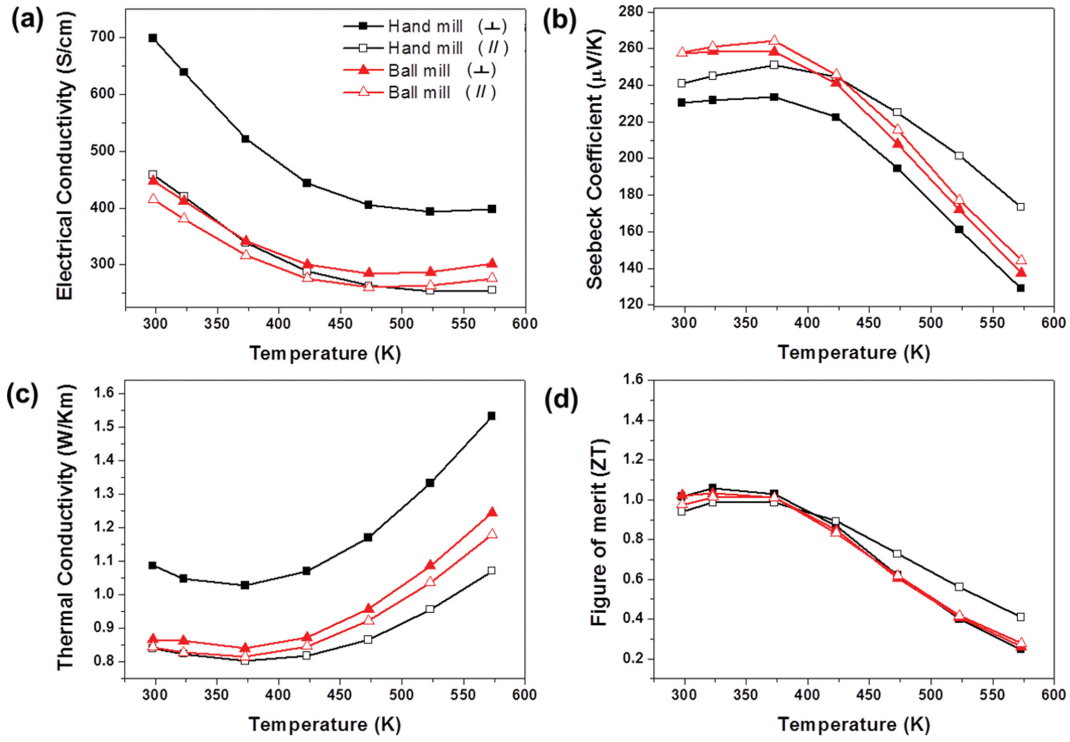

Fig. 7. Thermoelectric properties of sintered Bi-Sb-Te bulk pellets prepared from hand-milled and ball-milled powders.

tion perpendicular to the pressure. This direction dependency comes from their crystallographic orientation. Bi-Sb-Te has a hexagonal anisotropic crystal structure. Due to the van der Waals plane in c axis direction, the electrical and thermal conductivity in c-axis direction are lower than that of other directions. Ball-milled particles are large, so the crystal information is intact. The crystals are oriented along the sintering direction, showing anisotropic property. By contrast, bulk pellets fabricated using ball-milled powder show uniform electrical and thermal conductivity, regardless of measurement direction. The Seebeck coefficients for the two types of pellets prepared from the hand- and ball-milled powders were not much different. One notable point is that the ball-milled samples show higher Seebeck values at lower temperatures. The figure of merit, ZT, was also similar for the two pellets because electrical conductivity and thermal conductivity cancel each other out in the pellets prepared from hand-milled powder [21]. Although the overall ZT values were not dramatically improved by milling, the reduction of electrical and thermal conductivities was clearly observed, and anisotropic characteristics were removed.

CONCLUSIONS

The present study focused on the high-energy ball milling of Bi-Sb-Te material and described the grinding, agglomeration, and welding processes of the material during ball milling. Although Bi-Sb-Te materials are known to be brittle rather than ductile, they exhibit some ductile properties, such as the agglomeration and welding of small particles, owing to continuous mechanical milling and possibly because of cumulative heat generation during high-energy ball milling; consequently, the particle size increases. The inclusion of a secondary ball milling step with smaller balls and a lower speed was effective for obtaining uniform powders. Further, when the ball-milled powder was sintered, the resulting pellets showed no crystallographic orientation. Consequently, they exhibited uniform thermal and electrical conductivities regardless of measurement direction, in contrast with sintered pellets fabricated using the hand-milled powder.

ACKNOWLEDGEMENT

This work was supported by the National Research Foundation of Korea (NRF) grant funded by the Korea government (MSIT) (No. 2021R1A2C1011317).

REFERENCES

1. J. R. Sootsman, D. Y. Chung and M. G. Kanatzidis, *Angew. Chem. Int. Ed.*, **48**, 8616 (2009).
2. A. J. Minnich, M. S. Dresselhaus, Z. F. Ren and G. Chen, *Energy Environ. Sci.*, **2**, 466 (2009).
3. G. J. Snyder and E. S. Toberer, *Nat. Mater.*, **7**, 105 (2008).
4. G. G. Yadav, J. a. Susoreny, G. Zhang, H. Yang and Y. Wu, *Nanoscale*, **3**, 3555 (2011).
5. C. J. Vineis, A. Shakouri, A. Majumdar and M. G. Kanatzidis, *Adv. Mater.*, **22**, 3970 (2010).
6. B. Poudel, Q. Hao, Y. Ma, Y. Lan, A. Minnich, B. Yu, X. Yan, D. Wang, A. Muto, D. Vashaee, X. Chen, J. Liu, M. S. Dresselhaus, G. Chen and Z. Ren, *Science*, **320**, 634 (2008).
7. G. Lee, D. Lee and G. Ha, *Met. Mater. Int.*, **17**, 245 (2011).
8. W. Ren, C. Cheng, Z. Ren and Y. Zhong, *Physica B Condens. Matter*, **405**, 4931 (2010).
9. J. S. Chappell, T. A. Ring and J. D. Birchall, *J. Appl. Phys.*, **60**, 383 (1986).
10. M. S. Hossain, T. Li, Y. Yu, J. Yong, J.-H. Bahk and E. Skafidas, *RSC Adv.*, **10**, 8421 (2020).
11. F. Kim, B. Kwon, Y. Eom, J. E. Lee, S. Park, S. Jo, S. H. Park, B.-S. Kim, H. J. Im, M. H. Lee, T. S. Min, K. T. Kim, H. G. Chae, W. P. King and J. S. Son, *Nat. Energy*, **3**, 301 (2018).
12. A. Mostafaei, P. R. D. Vecchis, I. Nettleship and M. Chmielus, *Mater. Des.*, **162**, 375 (2019).
13. H. Wu, Y. Cheng, W. Liu, R. He, M. Zhou, S. Wu, X. Song and Y. Chen, *Ceram. Int.*, **42**, 17290 (2016).
14. A. Kanatzia, C. Papageorgiou, C. Lioutas and T. Kyratsi, *J. Electron. Mater.*, **42**, 1652 (2013).
15. S.-S. Lin and C.-N. Liao, *J. Appl. Phys.*, **110**, 093707 (2011).
16. J. H. Son, M. W. Oh, B. S. Kim, S. D. Park, B. K. Min, M. H. Kim and H. W. Lee, *J. Alloys Compd.*, **566**, 168 (2013).
17. C. Suryanarayana, *Prog. Mater Sci.*, **46**, 1 (2001).
18. J. Y. Huang, Y. K. Wu and H. Q. Ye, *Mater. Sci. Eng. A*, **199**, 165 (1995).
19. J. Lee, J. Kim, S.-Y. Lim, J.-Y. Kwon, J. Im, S.-M. Lee and S. E. Moon, *Electron. Lett.*, **53**, 930 (2017).
20. X. Chen, L. Liu, Y. Dong and L. Wang, *Prog. Nat. Sci. Mater. Int.*, **22**, 201 (2012).
21. J. J. Shen, L. P. Hu, T. J. Zhu and X. B. Zhao, *Appl. Phys. Lett.*, **99**, 124102 (2011).